THE JOURNAL OF BIOLOGICAL CHEMISTRY VOL. 286, NO. 30, pp. 26319–26326, July 29, 2011

Inhibition of RNase L and RNA-dependent Protein Kinase (PKR) by Sunitinib Impairs Antiviral Innate Immunity*

Received for publication, April 20, 2011, and in revised form, June 1, 2011 Published, JBC Papers in Press, June 2, 2011, DOI 10.1074/jbc.M111.253443

Babal Kant Jha[‡], Irina Polyakova[‡], Patricia Kessler[‡], Beihua Dong[‡], Benjamin Dickerman[§], Ganes C. Sen[§], and Robert H. Silverman[‡1]

From the Departments of [‡]Cancer Biology and [§]Molecular Genetics, Lerner Research Institute, Cleveland Clinic, Cleveland, Ohio 44195

RNase L and RNA-dependent protein kinase (PKR) are effectors of the interferon antiviral response that share homology in their pseudokinase and protein kinase domains, respectively. Sunitinib is an orally available, ATP-competitive inhibitor of VEGF and PDGF receptors used clinically to suppress angiogenesis and tumor growth. Sunitinib also impacts IRE1, an endoplasmic reticulum protein involved in the unfolded protein response that is closely related to RNase L. Here, we report that sunitinib is a potent inhibitor of both RNase L and PKR with IC_{50} values of 1.4 and 0.3 μM, respectively. In addition, flavonol activators of IRE1 inhibited RNase L. Sunitinib treatment of wild type (WT) mouse embryonic fibroblasts resulted in about a 12-fold increase in encephalomyocarditis virus titers. However, sunitinib had no effect on encephalomyocarditis virus growth in cells lacking both PKR and RNase L. Furthermore, oral delivery of sunitinib in WT mice resulted in 10-fold higher viral titers in heart tissues while suppressing by about 2-fold the IFN-β levels. In contrast, sunitinib had no effect on viral titers in mice deficient in both RNase L and PKR. Also, sunitinib reduced mean survival times from 12 to 6 days in virus-infected WT mice while having no effect on survival of mice lacking both RNase L and PKR. Results indicate that sunitinib treatments prevent antiviral innate immune responses mediated by RNase L and PKR.

RNase L and PKR[2] are host enzymes of higher vertebrates that participate in innate immunity against viral infections (1–4). Activation of both RNase L and PKR is triggered by the viral pathogen-associated molecular pattern, double-stranded RNA (dsRNA). However, whereas dsRNA directly binds to and activates PKR, in the case of RNase L activation is indirect. Interferon (IFN) treatment of cells induces PKR that, upon binding to dsRNA, phosphorylates first itself and then EIF2α thus blocking protein synthesis among other effects. RNase L degrades single-stranded RNA resulting in pleiotropic antiviral effects (5). Short 5′-triphosphorylated, 2′,5′-oligoadenylates (2–5A) are produced from ATP when viral dsRNA stimulates IFN-inducible oligoadenylate synthetases. 2–5A binds ankyrin repeats 2 and 4 in the N-terminal region of RNase L causing its dimerization and activation (6). RNase L is also pseudokinase with amino acid sequence homology to the PKR kinase domains (7).

IRE1, a kinase and endoribonuclease involved in the unfolded protein response, is another relative of RNase L (8). IRE1 spans the endoplasmic reticulum (ER) membrane. The intralumenal domains of IRE1 directly or indirectly sense unfolded proteins in the ER leading to autophosphorylation and ribonuclease activities in the cytoplasmic domains. IRE1 excises an intron from pre-mRNA for a transcription factor (HAC1 in yeast and XBP1 in mammals) leading to splicing and translation (9). HAC1/XBP1 drives expression of ER chaperones and protein folding enzymes that re-establish ER function. The kinase-extension-nuclease (KEN) domains of RNase L and IRE1 are highly homologous (8, 10, 11). However, although IRE1 is functional kinase, RNase L has dispensed with phosphoryl transfer activity (12). Nevertheless, residues involved in ATP binding are conserved in RNase L as well as in PKR (Table 1). In addition, ADP has a stimulatory effect on RNase L activity in the presence of 2–5A (13).

Kinase homology between RNase L, PKR, and IRE1 suggested to us that a compound that regulates one enzyme might affect all three. Sunitinib, a kinase inhibitor of VEGF-R and PDGF-R used clinically to suppress angiogenesis in cancer patients (14), activates yeast IRE1 (11) but inhibits human IRE1α (15). Here, we investigated the effects of sunitinib on RNase L and PKR in the context of antiviral innate immunity *in vivo*. In addition, we investigated flavonols, such as quercetin, that activate yeast IRE1 by binding at the dimer interface (Q site) in the IRE1 KEN domain (16). We also report that flavonols inhibit, rather than activate, RNase L.

EXPERIMENTAL PROCEDURES

Reagents, Antibodies, and Chemicals—Chemicals, unless stated otherwise, were analytical grade from Sigma. Sunitinib was obtained either from LC Laboratories, Woburn, MA or from Pfizer, Inc., New York. Poly(rI)·poly(rC) was from Calbiochem. Antibodies against PKR, phosphorylated PKR, EIF2α, and phosphorylated EIF2α were from Cell Signaling, Inc. (Danvers, MA). Monoclonal antibody against glutathione *S*-transferase was from BioLegend Inc. (San Diego). HPLC columns were from Dionex (Chelmsford, MA). The Äkta purifier and all columns and accessories were from GE Healthcare.

* This work was supported, in whole or in part, by National Institutes of Health Grants CA044059 (to R. H. S.) and CA062220 (to G. S.) from NCI.

[1] To whom correspondence should be addressed: Cleveland Clinic, 9500 Euclid Ave., NB40, Cleveland, OH 44195. Fax: 216-445-6269; E-mail: silverr@ccf.org.

[2] The abbreviations used are: PKR, RNA-dependent protein kinase; dsRNA, double-stranded RNA; EMCV, encephalomyocarditis virus; 2–5A, 2′,5′-oligoadenylate; ER, endoplasmic reticulum; MEF, mouse embryonic fibroblast; -R, receptor; KEN, kinase-extension-nuclease; DMS, dimethyl suberimidate; SPR, surface plasmon resonance.

TABLE 1
Residues involved in ATP binding in IRE1 KEN domain are conserved in PKR and RNase L

Residue in yeast IRE1	Interaction	Residue in RNase L	Residue in PKR	Conserved in RNase L	Conserved in PKR
Lys-702	H-bond	Lys-392	Lys-357	+	+
Leu-745	van der Waals	Val-434[a]	Met-366[a]	−	−
Glu-746	H-bond	Thr-435	Glu-367	−	+
Cys-748	H-bond	Cys-437	Cys-369	+	+
Asn-751	H-bond	Thr-440	Gly-372	−	−
Leu-804	van der Waals	Leu-492	Leu-492	+	+
Asp-828	H-bond	Asp-504	Asp-503	+	+

[a] The equivalent amino acid substitution can mimic the interaction.

Cell Lines and Mice—WT, *Rnasel*$^{-/-}$, *Pkr*$^{-/-}$, and *Rnasel*$^{-/-}$ *Pkr*$^{-/-}$ mice, all on C57/Bl6 background, were described previously (17–19). Mouse embryonic fibroblasts (MEF) were transformed with SV40 large T antigen. The human ovarian carcinoma cell line, Hey1b, was a kind gift from A. Marks (Toronto, Ontario, Canada) (20). Cells were cultured in RPMI 1640 medium with 10% fetal bovine serum (FBS).

Expression and Purification of RNase L—RNase L was purified as described previously (21) with modifications. Untagged recombinant human RNase L was expressed from baculovirus vector pFastBac1 in SF21 insect cells. Suspension cultures of SF21 cells were grown in SFM-II 900 insect cell medium (Invitrogen) supplemented with 10% FBS to a density of 1.5–2.0 × 10^6 cells/ml. Cells were infected at a multiplicity of infection of 5 at 27 °C, further grown for 72 h, and harvested by centrifugation at 1500 × *g*. Cell pellets were washed twice with chilled phosphate-buffered saline (PBS), resuspended in lysis buffer A (20 mM HEPES, pH 7.4, 5 mM $MgCl_2$, 50 mM KCl, 1 mM EDTA, 10% glycerol, 7.1 mM 2-mercaptoethanol, 2 μg/ml leupeptin, 2 μg/ml pepstatin, 50 μM phenylmethylsulfonyl fluoride (PMSF)), and disrupted using a French press at 1000–1500 p.s.i. Supernatants were collected after centrifugation at 100,000 × *g* for 1 h. The clarified lysates were incubated with a 25-ml bed volume of CL6B Blue-Sepharose affinity resin for 1 h at 4 °C. The protein-bound affinity resin was washed four times with 2 bed volumes each of buffer A and packed into an HR 16/26 column interfaced with an ÄKTA purifier UPC 10. The bound RNase L was eluted with a 0–1 M linear gradient of NaCl in buffer A over a period of 1 h at a flow rate of 1 ml/min. The peak fractions containing RNase L were pooled and desalted in buffer A. Desalted peak fractions were loaded onto a Mono Q HR 10/10 column, washed to attain a stable base line, and eluted with a 10–60% gradient of buffer B (buffer A plus 1 M NaCl) in 60 min at a flow rate of 1 ml/min. The purity of RNase L was >95%, as determined by SDS-PAGE and staining with Coomassie Blue.

Expression and Purification of Constitutively Active Mutant RNase $L_{N\Delta 335}$—A constitutively active N-terminally truncated RNase L, RNase $L_{N\Delta 335}$, was cloned and expressed as GST-tagged protein in pGST-parallel-2 and purified using glutathione-Sepharose as reported previously (22) with modifications. The plasmid $RL_{N\Delta 335}$-pGST-parallel-2 was expressed in BL21DE3pLysS bacteria. A single colony was inoculated in 50 ml of LB containing 2% glucose and grown overnight at 37 °C, 250 rpm. The overnight cultures were inoculated in fresh LB containing 100 μg/ml ampicillin (no glucose) at 10 ml/liter and grown at 37 °C, 250 rpm until the $A_{600\ nm}$ reached 0.6 arbitrary units. The bacterial cultures were cooled on ice, induced using 0.1 mM isopropyl 1-thio-β-D-galactopyranoside, and further grown for 16 h at 22 °C. Cells were harvested and washed twice with chilled Tris-buffered saline (TBS) and lysed in CelLytic™ B cell lysis reagent (Sigma) supplemented with 5 mM 2-mercaptoethanol, 0.5 μg/ml lysozyme, 5 units/ml benzonase, and protease inhibitor mixture (Roche Applied Science). Lysates were clarified by centrifugation and loaded on a GSTPrep FF16/60 column interfaced with an ÄKTA purifier UPC 10. The column was washed with buffer C (20 mM Tris-HCl, pH 8.0, 150 mM NaCl, 10% glycerol, 5 mM 2-mercaptoethanol) until a stable base line was achieved. The bound GST-tagged RNase $L_{N\Delta 335}$ was eluted with 20 mM reduced glutathione in buffer C in a one-step gradient over 5 column volumes. The fractions were analyzed by SDS-PAGE, and peak fractions (>90% purity) were pooled and loaded on a Sephacryl S 200 HR 26 mm × 100 cm size exclusion column and eluted in buffer A. Peak fractions were pooled and concentrated using Centriprep MWCO of 15-kDa centrifugal filter units and stored at −80 °C in aliquots.

Expression and Purification of PKR—Full-length human PKR cDNA cloned in a bi-cistronic bacterial expression vector, pET15b-hPKR-λ phosphatase, was expressed in BL21DE3pLysS bacteria (Novagen, EMD Chemicals, Gibbstown, NJ). A single colony of BL21DE3pLysS bacteria expressing pET15b-hPKR-λ phosphatase was inoculated in 50 ml of Luria Broth (LB) containing 2% glucose and grown overnight at 37 °C, 250 rpm. The overnight cultures were inoculated in 10 ml/liter fresh LB containing 100 μg/ml ampicillin (without glucose) and further grown at 37 °C, 250 rpm until the $A_{600\ nm}$ reached 0.7 arbitrary units. The bacterial culture was cooled on ice, induced using 1 mM isopropyl 1-thio-β-D-galactopyranoside, and further grown for 4 h at 23 °C. Cells were harvested and washed twice with chilled TBS, pH 7.5, and resuspended in lysis buffer D (20 mM Tris-HCl, pH 8.0, 500 mM NaCl, 10% glycerol, 5 mM 2-mercaptoethanol) supplemented with 0.2% Nonidet P-40, protease inhibitor mixture (Roche Applied Science) plus 5 units/ml benzonase. The resuspended cells were freeze-thawed twice followed by brief sonication. Lysates were clarified by centrifugation and loaded on a HisPrep 16/60 column interfaced with an ÄKTA purifier UPC 10. The column was washed with 20 column volumes of buffer D followed by 10 mM imidazole in buffer D until a stable base line was achieved. The bound hexahistidine-tagged PKR was eluted with imidazole linear gradient (10–250 mM) in buffer D, 10 column volumes. The fractions were analyzed by SDS-PAGE, and peak fractions (>90% purity) were pooled and loaded onto a Sep-

hacryl S 200 HR 16 mm × 100 cm size exclusion chromatography column in buffer E (20 mM HEPES, pH 7.5, 150 mM NaCl, 10% glycerol, and 5 mM β-mercaptoethanol). Peak fractions were pooled and concentrated using Centriprep MWCO 15-kDa centrifugal filter units (Millipore Inc., Billerica, MA) and stored at −80 °C in aliquots.

Synthesis and Purification of 5′-Triphosphoryl, 2′–5′-Linked Oligoadenylates (2–5A)—2–5A ($p_3(A2'p)_nA$, where $n = 1$ to ≥3) was enzymatically synthesized from ATP using hexahistidine-tagged and purified recombinant porcine 42-kDa 2–5A synthetase (a generous gift from Rune Hartmann, Aarhus, Denmark) (23). Individual 2–5A oligomers were purified (>98% purity) using a Dionex PA100 22 × 250 mm semi-preparative column interfaced with a Beckman system gold HPLC system under the control of 32-Karat™ workstation (24).

Fluorescence Resonance Energy Transfer (FRET) Assays—FRET assays were used to measure RNase L activity (25–27). Briefly, recombinant human RNase L (24 nM) or its constitutively active variant, RNase $L_{N\Delta335}$ (27), was incubated with varying concentrations of 2–5A, sunitinib, or flavonols. RNase L was preincubated with flavonols or sunitinib for 5 min on ice followed by the addition of 2–5A and a FRET probe (100 nM) in Cleavage buffer (25 mM Tris-HCl, pH 7.4, 100 mM KCl, 10 mM $MgCl_2$, and 7 mM 2-mercaptoethanol) for 10 min on ice and incubated for 60 min at 22 °C. The FRET probe is a 36-nucleotide synthetic oligoribonucleotide with a fluorophore (6-FAM™) at the 5′ terminus and a quencher (black hole quencher-1) at the 3′ terminus derived from the intergenic region of respiratory syncytial virus genomic RNA. The FRET RNA probe is highly susceptible to cleavage by RNase L because of the multiplicity of cleavage sites (UU or UA), 6-FAM™-UUA UCA AAU UCU UAU UUG CCC CAU UUU UUU GGU UUA-BHQ-1. In its uncleaved state, the fluorophore is in proximity to the quencher, and hence there is no emission due to FRET pairing. However, RNase L activation leads to the cleavage of the RNA probe, which separates the fluorophore and quencher. This cleavage of the FRET probe was monitored by excitation at 485 nm and emission at 535 nm using a Victor-2 multiplate reader (PerkinElmer Life Sciences). Each experiment was performed in triplicate, and data were plotted using GraphPad Prism.

Surface Plasmon Resonance (SPR)—Kinetic characterization of sunitinib binding was performed by SPR with a Biacore 3000 (GE Healthcare). Response units, a measure of binding, were monitored as a function of time. Purified anti-GST monoclonal antibody clone P1A12 (BioLegend Inc., San Diego) was immobilized on sensor CM5 chips (GE Healthcare) to achieve a base line gain of <400 response units. The purified GST-tagged RNase $L_{N\Delta335}$ (200 ng/ml) in buffer A supplemented with 0.005% surfactant P20 (SPR buffer) was immobilized on a sensor chip at a flow rate of 10 μl/min for 3 min at 25 °C to achieve a resonance response of 450–500 response units. An additional wash for 5 min at a flow rate of 20 μl/min was performed with buffer alone. Sunitinib (>99%, HPLC-purified, LC Laboratories) was dissolved in DMSO at 20 mM and diluted to working concentrations of 20, 10, 5 and 1 μM in SPR buffer HBS-P (GE Healthcare). Sunitinib solutions of different concentrations were passed over the sensor chip with immobilized GST-RNase $L_{N\Delta335}$ at a flow rate of 10 μl/min for 3 min, and association was monitored. Dissociation was monitored using SPR buffer for an additional 5 min. Data normalization against a reference channel immobilized with GST alone, analysis, and fitting was performed with BIAEvaluation software, version 3.2 (Biacore Inc.), with the option for simultaneous K_a/K_d calculations. Fitting of sensorgram data was carried out according to global fitting, and the K_a and K_d values were calculated with a 1:1 Langmuir model. In addition, these data were also used for independent K_d calculations by Scatchard plot analysis.

Ribosomal RNA (rRNA) Cleavage Assays—Effects of sunitinib on 2–5A-induced rRNA cleavage were monitored as described previously (28). Briefly, either Hey1b or MEF cells were plated. After 16 h, cells at about 60% confluency were treated with varying amounts of sunitinib for 3 h (Hey1b) or 2 h (MEF), and 2–5A was then transfected using Lipofectamine™ 2000 (Invitrogen). Thirty min after transfection, complete media with or without sunitinib were added. Cells were incubated for 5 h after which total RNA was isolated using TRIzol™ (Invitrogen) and resolved on RNA chips using an Agilent 2100 BioAnalyzer.

Chemical Cross-linking of RNase L with Dimethyl Suberimidate (DMS)—Chemical cross-linking of 2–5A-induced dimers of purified recombinant human RNase L was performed in the presence or absence of sunitinib as reported with modifications (22, 29). The purified RNase L (1.4 mg/ml) was dialyzed three times against an ~500-ml volume of buffer A at 4 °C for 16 h. Five μl of 0.5 μM RNase L was incubated in the presence or absence of 10 μM sunitinib with or without 100 μM ADP for 30 min on ice. 2–5A was added to a final concentration of 5 μM and further incubated for 2 h. To obtain cross-linking, DMS in 0.4 M triethanolamine, pH 8.5, was added to a final concentration of 4 mg/ml and incubated for additional 2 h on ice. RNase L was denatured by adding loading buffer (Novagen, EMD Chemicals, Gibbstown, NJ) and heating at 95 °C for 5 min. Proteins were separated by 10% SDS-PAGE, transferred to nitrocellulose membranes, probed with 1:5000 dilution of monoclonal antibodies against RNase L (22) followed with goat anti-mouse IgG-peroxidase (Cell Signaling, Danvers, MA), and developed with enhanced chemiluminescence (GE Healthcare).

PKR Assays—Recombinant purified human PKR at 10 μg/ml was incubated with varying concentrations of sunitinib on ice for 30 min in buffer F (20 mM Tris-HCl, pH 7.5, 50 mM KCl, 5% glycerol, 2 mM $MgCl_2$, and 2 mM $MnCl_2$) followed by the addition of 200 ng/ml (final concentration) of poly(rI)·poly(rC) and 10 μCi of [γ-^{32}P]ATP. The mixtures, in a final volume of 50 μl, were incubated for 20 min at 30 °C, stopped by heating the sample in SDS-PAGE loading buffer at 95 °C for 3 min, and resolved by 10% SDS-PAGE. Gels were fixed in 10% acetic acid, 50% methanol for 10 min followed by five washes in water and dried. The dried gels were placed with a phosphor screen and scanned on Storm 840 variable mode imager (GE Healthcare). The data fitting and analysis was performed using nonlinear regression in GraphPad Prizm.

Monitoring EIF2α Phosphorylation—MEF were seeded at 60% confluence, grown for 16 h, and treated with the indicated amounts of sunitinib for 2 h. A 2 μg/ml final concentration of poly(rI)·poly(rC) was transfected using Lipofectamine 2000 and

incubated for 2 h in the presence or absence of sunitinib. The cells were harvested in Nonidet P-40 lysis buffer (50 mM Tris-HCl, pH 7.2, 0.15 M NaCl, 1% Nonidet P-40, 200 μM sodium orthovanadate, 2 mM EDTA, and 5 mM DTT). Protein amounts were estimated using the Bradford method (Bio-Rad), and 25 μg of total protein was separated on 10% SDS-PAGE, transferred onto nitrocellulose membranes, and probed with either antibody against total anti-EIF2α or Ser-51-phosphorylated EIF2α.

Viral Growth Assays in MEF—MEF were plated at 60–70% confluence and grown overnight. The MEF were then pretreated with sunitinib for 2 h and infected with encephalomyocarditis virus (EMCV) at a multiplicity of infection of 0.05 in RPMI 1640 medium containing 2% serum. After 1 h the supernatants were removed; cells were washed at room temperature with PBS, and fresh complete RPMI 1640 media with 10% FBS with or without 5 μM sunitinib was added. Cells were incubated for 6 h in a humidified CO_2 incubator at 37 °C. Media containing virus were harvested, and serial 10-fold dilutions were used to infect the indicator cell line, L929. After a 1-h viral adsorption step, cells were washed and incubated for 16 h in plaquing media (1% carboxymethylcellulose in DMEM containing 10% FBS) (26). The media were removed, and cells were fixed with 10% formaldehyde in PBS and stained using 0.1% crystal violet. The plaques were counted, and data were analyzed.

Animal Experiment—All mouse experiments were performed according to institutional guidelines at the Cleveland Clinic, Lerner Research Institute, under a protocol approved by the Institutional Animal Care and Use Committee. Wild type (WT) mice and *Rnasel*$^{-/-}$, *Pkr*$^{-/-}$, and *Rnasel*$^{-/-}$ *Pkr*$^{-/-}$ mice (all on a genetic background of C57/bl6) at 9–16 weeks of age received daily treatments with 50 μl of either PBS or sunitinib (20 mg/kg body weight) by oral gavage beginning 2 days prior to infection and continuing until the mice were sacrificed. Infections were with EMCV (2000 plaque-forming units (pfu)/kg) by the intraperitoneal route. To determine the viral titers in heart tissue, virus-infected mice were monitored at least twice daily and sacrificed at 96 h post-infection. For animal survival experiments, virus-infected mice were sacrificed when death was imminent. All virus infections and treatments were performed in an animal bio-safety level 2 laboratory (ABSL2).

For viral growth assays, mice were sacrificed at 96 h, and heart tissues and blood were harvested and processed. Hearts were perfused with PBS and homogenized using a Sample Grinding kit (GE Healthcare). The tissue homogenates were centrifuged at 1000 × *g* for 15 min at 4 °C in a swinging bucket rotor. The supernatants were collected and used for plaque assays on the indicator cell line L929 (26).

IFN-β ELISA—IFN-β levels were measured in mouse serum using a mouse IFN-β ELISA kit (Pestka Biomedical Laboratories, Inc., Piscataway, NJ).

RESULTS

Sunitinib Inhibits RNase L Activity—A FRET-based assay was used to monitor RNase L activity (25). Trimer 2–5A ($p_3$5′A2′p5′A2′p5′A) potently activated RNase L with an EC_{50} of 0.2 nM (Fig. 1*A*). In contrast, sunitinib inhibited RNase L activity measured in the presence of 2–5A (Fig. 1*B*). The IC_{50} (50% inhibition of enzyme activity at a saturating concentration of 2–5A) for sunitinib was determined by nonlinear regression analysis to be 1.4 μM. A constitutively active N-terminal deletion mutant form of RNase L (NΔ335) (27) that lacks the 2–5A binding domain was similarly inhibited by sunitinib (IC_{50} = 0.5 μM). RNase L activity was also determined in intact human (Hey1b) and MEF cell lines by monitoring highly specific and characteristic cleavages in rRNA in intact ribosomes (30). Cells were treated with sunitinib for 2 h prior to transfection with trimer 2–5A for 5 h. RNase L activation was completely prevented by pretreatment with 5 μM of sunitinib in both cell lines (Fig. 1, *C* and *D*). However, partial inhibition of RNase L activity was apparent at concentrations of sunitinib as low as 1 μM.

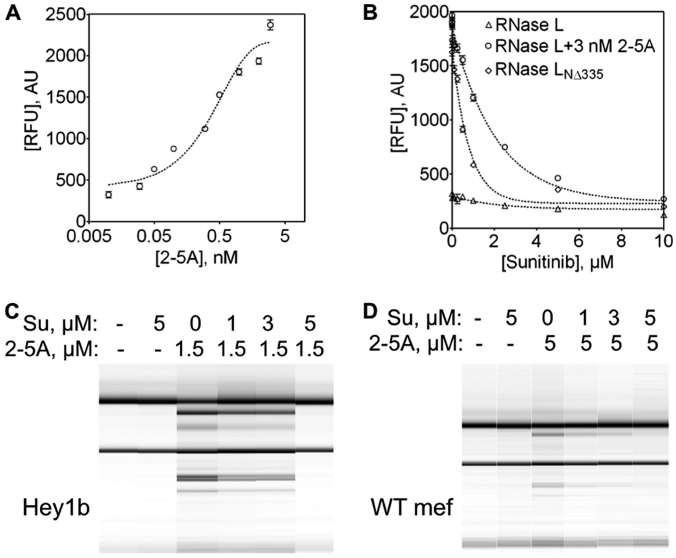

FIGURE 1. **Sunitinib inhibits RNase L.** *A,* RNase L activation by pppA2′p5′A2′p5′A (2–5A) was determined by FRET as described under "Experimental Procedures." *B,* inhibition of RNase L (24 nM) and RNase $L_{N\Delta335}$ (0.5 μM) by sunitinib. *RFU*, relative fluorescence units. *C* and *D,* inhibition of RNase L by sunitinib in Hey1b cells (*C*) and MEF (*D*) as determined by monitoring rRNA cleavage following transfection with 2–5A. *SU*, sunitinib; *AU*, arbitrary units.

Binding Affinity of Sunitinib to RNase L—To determine the affinity RNase L for sunitinib, we employed SPR ("Experimental Procedures"). There was no apparent binding of sunitinib by itself to the sensor chip under experimental conditions (data not shown). In contrast, the sensograms indicate concentration-dependent, steady-state binding of sunitinib to the RNase L KEN domain with rapid kinetics (Fig. 2*A*). The dissociation constant (K_d), 6.4 μM, was determined by Scatchard analysis using resonance at equilibrium and separately by global data analysis with BIAevaluation software (Fig. 2*B* and data not shown). The quality of the fit was determined by χ^2 values, as well as from the magnitude and distribution of the residuals (31).

Sunitinib Prevents RNase L Dimerization—2–5A binding causes RNase L dimerization coinciding with enzyme activation (22, 32). A missense mutation in the ATP-binding domain residue, K392R, in protein kinase-like domain II was previously shown to inhibit enzyme dimerization (12). Therefore, because sunitinib is an ATP competitor drug, we determined the effects of sunitinib on RNase L dimerization triggered by 2–5A (Fig. 3). As reported previously, addition of 2–5A induces RNase L

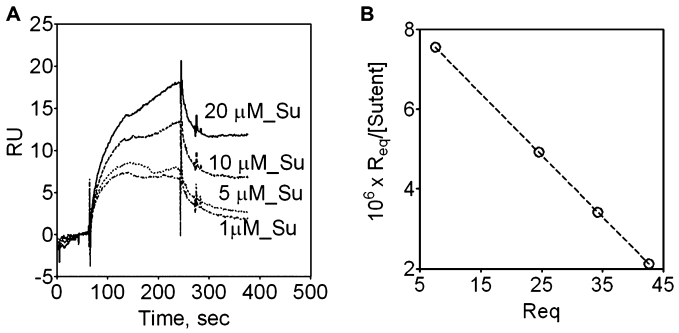

FIGURE 2. **Sunitinib binding to the KEN domain of RNase L determined by SPR.** *A,* sensograms of sunitinib binding with RNase $L_{N\Delta335}$ as a function of time with different amounts of sunitinib. *B,* Scatchard plot for binding of sunitinib to RNase $L_{N\Delta335}$. *RU,* response units; *SU,* sunitinib; *Req,* response unit at equilibrium.

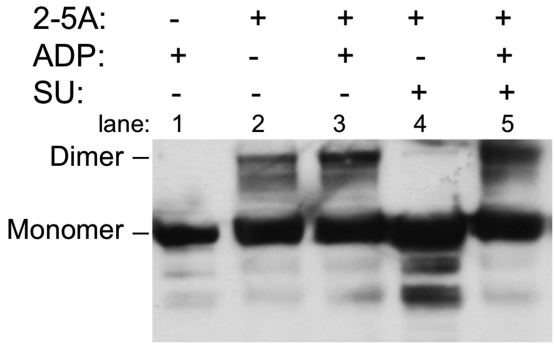

FIGURE 3. **Sunitinib inhibition of RNase L dimerization is prevented by ADP.** Chemical cross-linking of RNase L in the presence or absence of 2–5A (5 μM), ADP (100 μM), and sunitinib (10 μM) as indicated was performed using DMS as described under "Experimental Procedures." The cross-linked products were resolved on 10% SDS-PAGE followed by transfer on nitrocellulose membrane and probed with monoclonal antibody against RNase L.

dimerization as determined by protein-protein cross-linking with DMS (Fig. 3, compare *lanes 1* and *2*) (29). Although ADP alone did not cause dimerization, ADP enhanced dimerization induced by 2–5A (Fig. 3, compare *lanes 2* and *3*). Sunitinib (10 μM) completely prevented RNase L dimerization in response to 2–5A (Fig. 3, *lane 4*). However, a 10-fold molar excess of ADP prevented the inhibitory effect of sunitinib (Fig. 3, *lane 5*). Results suggest that the inhibitory effect of sunitinib is mediated through the ATP-binding pocket.

Flavonols Inhibit RNase L Activity—A prior study showed that flavonols, in particular, quercetin, activates the RNase activity of yeast IRE1 and potentiates stimulation by ADP (16). Because of homology between the RNase L and IRE1 KEN domains, we determined the effects of a number of different flavonol compounds on RNase L activity (Fig. 4 and Table 2). Remarkably, all of these flavonols, including quercetin, were inhibitors of RNase L activation by 2–5A, although the inhibition could be partially prevented by the addition of ADP. These findings suggest that the effect of the flavonols was mediated through the ATP binding domain of RNase L, similarly to the effect of sunitinib, and were therefore distinct from effects of flavonol on yeast IRE1.

Inhibition of PKR Activity by Sunitinib—Because of sequence homology between the kinase and kinase-like domains of PKR and RNase L, respectively, we reasoned that sunitinib might similarly inhibit PKR activity. Therefore, autophosphorylation

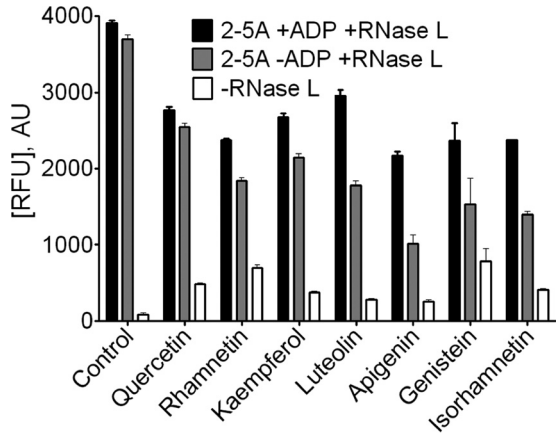

FIGURE 4. **Inhibition of RNase L activity by flavonols is partially prevented by ADP.** RNase L activity was determined by FRET assay as described under "Experimental Procedures," in the presence or absence of 3 nM 2–5A, flavonol compounds (as indicated) at 5 μM, and ADP (100 μM). The experiment was done in triplicate. Standard deviations are indicated. *AU,* arbitrary units; *RFU*, relative fluorescence units.

TABLE 2

IC_{50} values of flavonols on RNase L activity in the presence and absence of ADP (100 μM)

Compounds	IC_{50}, μM	
	− ADP	+ ADP
Quercetin	20	25
Rhamnetin	10	>50
Kaempferol	10	>10
Luteolin	12	>50
Apigenin	0.5	13.5
Genistein	4	22
Isorhamnetin	9	28

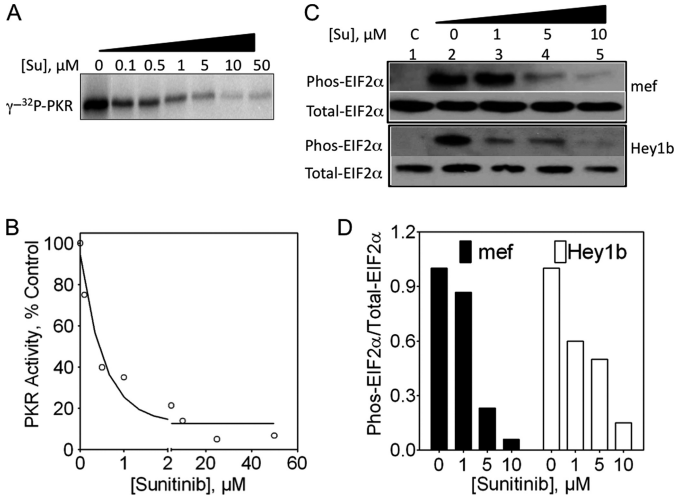

FIGURE 5. **Sunitinib inhibits PKR activity.** *A* and *B,* autophosphorylation of purified PKR in response to poly(rI)·poly(rC) is inhibited by sunitinib (*SU*). The data in *A* were analyzed using ImageQuant 2.0 and plotted in *B* by GraphPad Prism with nonlinear regression fit. *C* and *D*, phosphorylation of EIF2α in MEF and Hey1b cells in response to transfection with poly(rI)·poly(rC) is inhibited by sunitinib (*SU*). *Lane 1* was performed without poly(rI)·poly(rC). Results in *C* were analyzed using ImageJ (rsb.info.nih.gov) and presented as ratios of phosphorylated/total EIF2α in *D*. *Phos-EIF2α*, phosphorylated EIF2α.

of purified recombinant human PKR was monitored in the presence or absence of sunitinib after subsequent stimulation with poly(rI)·poly(rC) (Fig. 5*A*). A dose-dependent inhibition of PKR was obtained with increased concentrations of sunitinib. Sunitinib inhibited PKR with an IC_{50} of 0.3 μM (Fig. 5*B*).

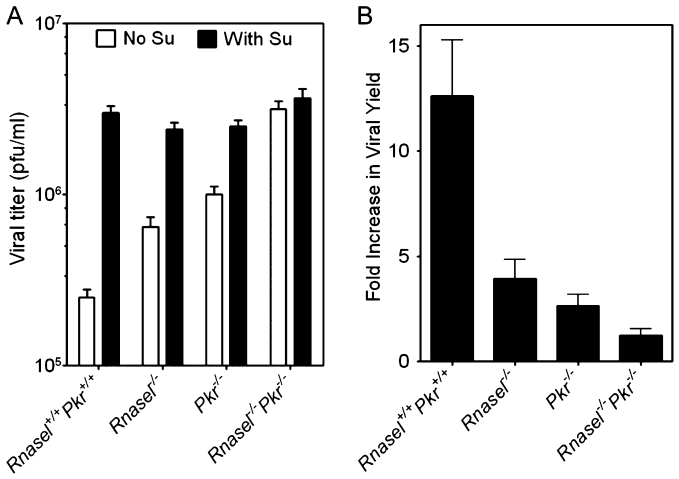

FIGURE 6. **Sunitinib enhances virus replication in MEF by inhibiting RNase L and PKR.** *A,* MEF cells of the indicated genotype were treated with 5 μM sunitinib (*Su*) for 2 h followed by EMCV infection for 6 h. Viral titers were determined by plaque assays ("Experimental Procedures"). *B,* results from *A* are presented as fold-increase in viral yield upon sunitinib treatment. Results are an average of two experiments done in triplicate.

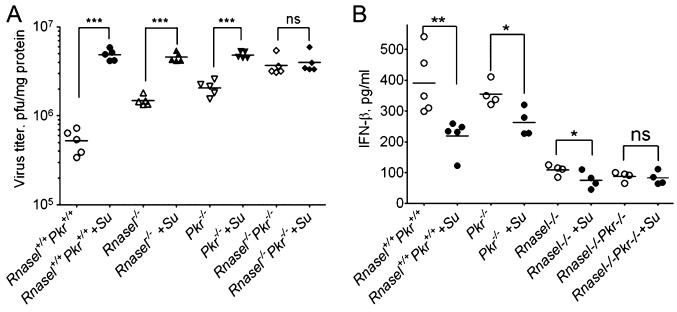

FIGURE 7. **Sunitinib treatments enhance viral replication *in vivo* while suppressing IFN-β induction.** *A,* groups of five mice of the indicated genotypes were treated with sunitinib (*Su*) (20 mg/kg/day) beginning 2 days prior to infection by oral gavage. Mice were inoculated with EMCV (2000 pfu/kg) by the intraperitoneal route, and viral titers in the heart at 96 h post-infection were determined by plaque assays. Viral yields (pfu/mg protein) are shown. *B,* IFN-β levels in sera were determined by ELISA in the same experiment at 96 h post-infection. The *horizontal lines* are the mean (IFN-β). Data analysis was performed in GraphPad Prism. The *p* values from Student's *t* tests are as follows: *, <0.05; **, <0.005.

Translational initiation factor EIF2α is one the principal substrates of PKR (reviewed in Ref. 4). Phosphorylation of EIF2α on serine 51 by PKR and related kinases (HRI, GCN2, and PERK) results in a cessation of protein synthesis because of a block in recycling of EIF2α bound to GDP. Pretreatment of cells for 2 h with sunitinib prior to transfection with poly(rI)·poly(rC) (to specifically activate PKR) inhibited phosphorylation of EIF2α with IC_{50} values of 4.4 and 4.9 μM in WT MEF and Hey1b cells, respectively (Fig. 5, *C* and *D*).

Sunitinib Inhibits the Antiviral Activities of RNase L and PKR—Because RNase L and PKR have antiviral activity, we reasoned that inhibition of both proteins by sunitinib should enhance virus replication. Therefore, the effect of sunitinib on virus replication was determined in MEF that were wild type (WT) or singly or doubly deficient for RNase L and PKR. MEF were pretreated with sunitinib for 2 h prior to infection with EMCV, a cardiovirus in the Picornaviridae family (Fig. 6). Sunitinib treatment led to a 12-fold increase in viral yield in the WT MEF, but only a 3.5- and 2.5-fold increase in MEF lacking RNase L or PKR, respectively. In contrast, sunitinib had no effect on viral yields in MEF doubly deficient for RNase L and PKR. These results indicate that sunitinib inhibition of RNase L and/or PKR in cells leads to enhanced virus replication.

Effect of Sunitinib Treatment on Antiviral Innate Immunity in Mice—To determine whether the pro-viral effect of sunitinib treatment could be demonstrated *in vivo*, viral infections were performed in mice in the presence or absence of sunitinib treatments. Sunitinib (20 mg/kg) was administered by oral gavage to WT ($Rnasel^{+/+}$ and $Pkr^{+/+}$), $Rnasel^{-/-}$ $Pkr^{+/+}$, $Rnasel^{+/+}$ $Pkr^{-/-}$, and $Rnasel^{-/-}$ $Pkr^{-/-}$ mice beginning 2 days prior to infection with daily treatments until the mice were sacrificed. Mice were infected with EMCV (2000 pfu/kg) and sacrificed at 4 days post-infection. The viral yields in the heart were determined by plaque assays (Fig. 7*A*). Sunitinib treatments increased viral yields in heart by 11-, 5-, and 4-fold in WT, RNase L-null, and PKR-null mice, respectively. However, in mice lacking both RNase L and PKR, there was no effect of sunitinib on virus replication in the heart.

Levels of IFN-β were determined by ELISA in the blood of these same mice as a measure of the innate immune response to infection (Fig. 7*B*). Basal levels of IFN-β in the absence of infections were <10 units/ml (data not shown). Virus-induced levels of IFN-β were slightly higher in WT mice (391 units/ml) than in PKR-deficient mice (351 units/ml) but about 4-fold higher than in mice lacking RNase L alone (109 units/ml) or lacking both RNase L and PKR (88 units/ml). Sunitinib treatment reduced viral induction of IFN-β by 1.8-, 1.3-, and 1.4-fold in the WT, PKR-null, and RNase L-null mice, respectively. However, there was no effect of sunitinib of IFN-β levels in the mice doubly deficient for both RNase L and PKR.

Sunitinib Enhances Viral Pathogenesis in WT Mice but Not in Mice Lacking RNase L and PKR—To determine whether sunitinib treatment affected viral pathogenesis, sunitinib-treated and control mice were infected with EMCV and monitored for moribund state as defined by huddled posture, ruffled fur, and inactivity. In untreated mice, median survival following EMCV infection was 12, 9, 8, and 9 days in the WT, RNase L-null, PKR-null, and RNase L-null/PKR-null, respectively (Fig. 8 and Table 3). Sunitinib treatments dramatically shortened median survival time in the WT mice from 12 to 6 days ($p = 0.005$) (Fig. 8 and Table 3). In contrast, sunitinib treatments reduced median survival time by 2 days in the RNase L-null mice ($p = 0.014$) and by 1 day in the PKR-null mice ($p = 0.015$). There was no effect of sunitinib on animal survival in mice lacking both RNase L and PKR. These findings suggest that inhibition of RNase L and PKR by sunitinib enhances viral replication and pathogenesis.

DISCUSSION

Inhibitory Effects of ATP-competitive Drugs on RNase L Activity—Here, we demonstrate that sunitinib, an ATP-competitive inhibitor of receptor tyrosine kinases, including PDGF-R and VEGF-R, is also an inhibitor of the serine/threonine kinase, PKR, and pseudokinase, RNase L. We used a highly specific and sensitive FRET assay *in vitro* to directly measure

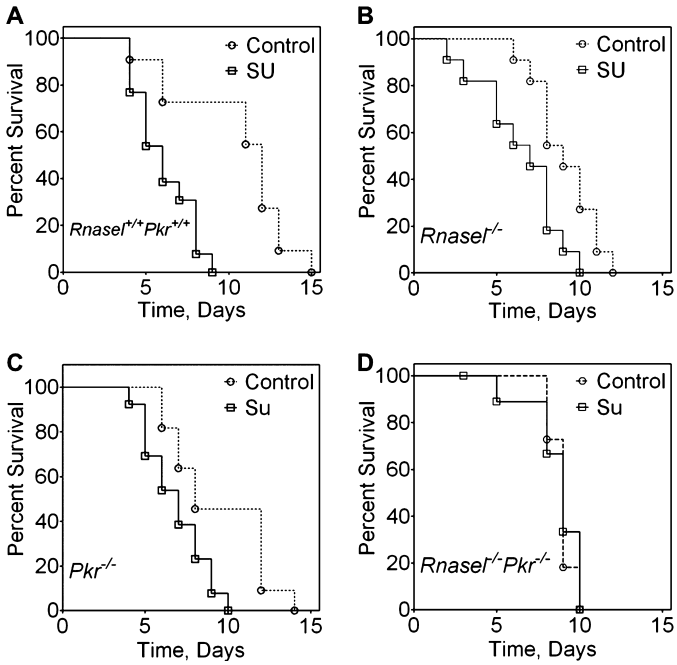

FIGURE 8. **Sunitinib treatments hasten death of mice from viral infections due to inhibition of RNase L and PKR.** *A–D,* mice of the indicated genotypes, untreated or treated with sunitinib (*Su*), were infected with EMCV as described in the legend to Fig. 7. Kaplan Meier survival curves in the absence or presence of sunitinib are shown.

TABLE 3
Effect of sunitinib treatments on animal survival from viral infection

Genotype	Median survival		*p* value
	Sunitinib (*n*)[a]	Control (*n*)[a]	
	days		
Rnasel$^{+/+}$ *Pkr*$^{+/+}$	6 (13)	12 (11)	0.005
Rnasel$^{-/-}$	7 (11)	9 (11)	0.014
Pkr$^{-/-}$	7 (13)	8 (11)	0.015
Rnasel$^{-/-}$ *Pkr*$^{-/-}$	9 (11)	9 (9)	0.77

[a] *n* = number of mice per group.

RNase L activity. A complete RNase L protein and an isolated KEN domain were both inhibited by sunitinib. Specific and characteristic cleavage of rRNA in intact ribosomes is a hallmark of RNase L activation in mammalian cells (30). We showed that sunitinib inhibition of RNase L prevented rRNA cleavage in intact human and mouse cells. Sunitinib specifically binds to the ATP binding pocket of several different protein kinases, including VEGFR2, PDGF-R2, FGFRβ1, and EGF-R (33). RNase L has a protein kinase-like domain, including conserved residues responsible for ADP/ATP binding. Sunitinib interacts with the KEN domain of RNase L, presumably through the ATP-binding pocket in the protein kinase domain II (12). Although ADP enhances RNase L activity in some instances (13), ADP/ATP is not required as a co-factor for RNase L activation by 2–5A (34). RNase L activation is a two-step process. First, 2–5A binds to N-terminal ankyrin repeats 2 and 4 of RNase L (6). Second, RNase L is believed to undergo a conformational change upon 2–5A binding in which protein-protein interaction domains are exposed, and the nuclease domain is thought to disassociate from an internal inhibitory domain (35). Hence, dimerization is an essential step in the activation of RNase L. Our protein-protein cross-linking data show that sunitinib effectively blocks the dimerization of RNase L. However, a 10-fold molar excess of ADP was able to prevent inhibition of dimerization by sunitinib. These results support the idea that sunitinib inhibition of RNase L occurs through the ADP/ATP-binding site of RNase L. These findings could be the first example of a pseudokinase that is inhibited by a kinase inhibitor.

Flavonols, such as quercetin, activate IRE1 because of interaction at a "Q site" at the dimer interface of the IRE1 KEN domain and not through the ATP-binding site. However, the Q site residues in yeast IRE1 are not conserved in RNase L. It was therefore of interest to determine the effect of quercetin and other flavonols on RNase L activity. Interestingly, flavonols inhibit, rather than activate, RNase L, effects that were partially prevented by a 20-fold molar excess of ADP. Therefore, flavonols have effects similar to sunitinib that are likely to be mediated through the ADP/ATP binding pocket of RNase L.

RNase L and IRE1 are highly similar in their KEN domains, although RNase L is a pseudokinase and IRE1 is a functional kinase (8, 12). A recent structure of the dephosphorylated KEN domain of human IRE1α is a face-to-face dimer that precedes the active back-to-back structure (15). Sunitinib is an inhibitor of both human IRE1α autophosphorylation and mRNA splicing, the latter effect catalyzed in part by the IRE1α RNase. Our results demonstrate similar effects of sunitinib on RNase L, an inhibition mediated through the ADP/ATP-binding site that blocks ribonucleolytic activity. In contrast, sunitinib is an activator, rather that an inhibitor, of yeast IRE1 (11).

Sunitinib Is a Novel Inhibitor of PKR—Sunitinib is shown here to be an effective inhibitor of the antiviral enzyme, PKR, in a cell-free system and in intact mammalian cells. Both PKR autophosphorylation and phosphorylation of EIF2α were potently suppressed by sunitinib treatment. Although we did not investigate the mechanism for the inhibition of PKR, the most likely explanation for the effect is competitive inhibition of binding of ATP substrate to the enzyme. We demonstrate using highly specific and selective *in vitro* as well as a cell culture model system that sunitinib is a potent inhibitor of both RNase L and PKR with IC_{50} values of 1.4 and 0.3 μM, respectively. These IC_{50} values are well within the range of earlier reported targets of sunitinib (36). For example sunitinib inhibits AKT1 and AMPK serine kinases with IC_{50} values of 3.8 and 0.2 μM, respectively (37). Conversely, the K_d values of sunitinib for VEGF-R and PDGF-R are in the nanomolar range, whereas the K_d value for PKR was 0.67 μM (36).

Sunitinib Treatments Enhance Viral Infections in Mice by Blocking RNase L and PKR—We show here that sunitinib inhibits RNase L and PKR and thus enhances viral growth in cultured cells and in mice. The proviral effect of sunitinib is observed only when RNase L and PKR are present. Indeed, viral yields in hearts of WT mice were about 10-fold greater when the animals received sunitinib orally. However, sunitinib had no effect on viral yields in mice lacking both RNase L and PKR. Viral induction of IFN-β was about 4-fold greater in WT mice than in mice lacking RNase L. The RNase L effect could be due to short RNA cleavage products that amplify IFN-β induction through RIG-I or MDA5 (5, 38, 39). In contrast, a deficiency in PKR had only a minimal effect on virus induction of IFN-β.

These results are consistent with a prior study in which the induction of type I IFN genes by poly(rI)·poly(rC) and virus was shown to be unimpaired in $Pkr^{-/-}$ mice (40). Sunitinib treatments reduced viral induction of IFN-β in the WT, $Rnasel^{-/-}$, and $Pkr^{-/-}$ mice but not in the $Rnasel^{-/-}$ $Pkr^{-/-}$ mice. However, levels of IFN-β were already very low in the double knock-out mice rendering these results difficult to interpret, especially given that sunitinib might affect other kinases involved in the induction of IFN-β. As shown here and in our previous studies, mice lacking either or both RNase L and PKR are at a higher risk of viral infection (17, 18).

In these studies, death from viral infection was dramatically hastened by sunitinib treatments. Remarkably, this occurred in WT mice but not in mice lacking both RNase L and PKR. An intermediate effect of sunitinib on animal survival was obtained in mice lacking only RNase L or only PKR. Our findings indicate an important role for the kinase-like domain, in particular the ATP-binding site, in the regulation of RNase L activity. In addition, sunitinib is shown to be a useful research reagent for suppressing both RNase L and PKR in cell culture experiments as well as in mice. The relevance of these studies to sunitinib use in humans is presently unknown, but results suggest that under some circumstances sunitinib treatments might increase the risk of viral infections.

Acknowledgments—We thank Brian Rini (Cleveland) for advice and Christina Gaughan for excellent technical assistance.

REFERENCES

1. Samuel, C. E. (2001) *Clin. Microbiol. Rev.* **14,** 778–809
2. Chakrabarti, A., Jha, B. K., and Silverman, R. H. (2011) *J. Interferon Cytokine Res.* **31,** 49–57
3. Silverman, R. H. (2007) *J. Virol.* **81,** 12720–12729
4. Sadler, A. J., and Williams, B. R. (2008) *Nat. Rev. Immunol.* **8,** 559–568
5. Malathi, K., Dong, B., Gale, M., Jr., and Silverman, R. H. (2007) *Nature* **448,** 816–819
6. Tanaka, N., Nakanishi, M., Kusakabe, Y., Goto, Y., Kitade, Y., and Nakamura, K. T. (2004) *EMBO J.* **23,** 3929–3938
7. Manning, G., Whyte, D. B., Martinez, R., Hunter, T., and Sudarsanam, S. (2002) *Science* **298,** 1912–1934
8. Dong, B., Niwa, M., Walter, P., and Silverman, R. H. (2001) *RNA* **7,** 361–373
9. Bernales, S., Papa, F. R., and Walter, P. (2006) *Annu. Rev. Cell Dev. Biol.* **22,** 487–508
10. Lee, K. P., Dey, M., Neculai, D., Cao, C., Dever, T. E., and Sicheri, F. (2008) *Cell* **132,** 89–100
11. Korennykh, A. V., Egea, P. F., Korostelev, A. A., Finer-Moore, J., Zhang, C., Shokat, K. M., Stroud, R. M., and Walter, P. (2009) *Nature* **457,** 687–693
12. Dong, B., and Silverman, R. H. (1999) *Nucleic Acids Res.* **27,** 439–445
13. Wreschner, D. H., Silverman, R. H., James, T. C., Gilbert, C. S., and Kerr, I. M. (1982) *Eur. J. Biochem.* **124,** 261–268
14. Kerbel, R. S. (2006) *Science* **312,** 1171–1175
15. Ali, M. M., Bagratuni, T., Davenport, E. L., Nowak, P. R., Silva-Santisteban, M. C., Hardcastle, A., McAndrews, C., Rowlands, M. G., Morgan, G. J., Aherne, W., Collins, I., Davies, F. E., and Pearl, L. H. (2011) *EMBO J.* **30,** 894–905
16. Wiseman, R. L., Zhang, Y., Lee, K. P., Harding, H. P., Haynes, C. M., Price, J., Sicheri, F., and Ron, D. (2010) *Mol. Cell* **38,** 291–304
17. Zhou, A., Paranjape, J., Brown, T. L., Nie, H., Naik, S., Dong, B., Chang, A., Trapp, B., Fairchild, R., Colmenares, C., and Silverman, R. H. (1997) *EMBO J.* **16,** 6355–6363
18. Zhou, A., Paranjape, J. M., Der, S. D., Williams, B. R., and Silverman, R. H. (1999) *Virology* **258,** 435–440
19. Leitner, W. W., Hwang, L. N., deVeer, M. J., Zhou, A., Silverman, R. H., Williams, B. R., Dubensky, T. W., Ying, H., and Restifo, N. P. (2003) *Nat. Med.* **9,** 33–39
20. Baumal, R., Law, J., Buick, R. N., Kahn, H., Yeger, H., Sheldon, K., Colgan, T., and Marks, A. (1986) *Cancer Res.* **46,** 3994–4000
21. Silverman, R. H., Dong, B., Maitra, R. K., Player, M. R., and Torrence, P. F. (2000) *Methods Enzymol.* **313,** 522–533
22. Dong, B., and Silverman, R. H. (1995) *J. Biol. Chem.* **270,** 4133–4137
23. Hartmann, R., Justesen, J., Sarkar, S. N., Sen, G. C., and Yee, V. C. (2003) *Mol. Cell* **12,** 1173–1185
24. Molinaro, R. J., Jha, B. K., Malathi, K., Varambally, S., Chinnaiyan, A. M., and Silverman, R. H. (2006) *Nucleic Acids Res.* **34,** 6684–6695
25. Thakur, C. S., Xu, Z., Wang, Z., Novince, Z., and Silverman, R. H. (2005) *Methods Mol. Med.* **116,** 103–113
26. Thakur, C. S., Jha, B. K., Dong, B., Das Gupta, J., Silverman, K. M., Mao, H., Sawai, H., Nakamura, A. O., Banerjee, A. K., Gudkov, A., and Silverman, R. H. (2007) *Proc. Natl. Acad. Sci. U.S.A.* **104,** 9585–9590
27. Dong, B., and Silverman, R. H. (1997) *J. Biol. Chem.* **272,** 22236–22242
28. Malathi, K., Paranjape, J. M., Ganapathi, R., and Silverman, R. H. (2004) *Cancer Res.* **64,** 9144–9151
29. Davies, G. E., and Stark, G. R. (1970) *Proc. Natl. Acad. Sci. U.S.A.* **66,** 651–656
30. Wreschner, D. H., James, T. C., Silverman, R. H., and Kerr, I. M. (1981) *Nucleic Acids Res.* **9,** 1571–1581
31. Myszka, D. G. (1997) *Curr. Opin. Biotechnol.* **8,** 50–57
32. Carroll, S. S., Cole, J. L., Viscount, T., Geib, J., Gehman, J., and Kuo, L. C. (1997) *J. Biol. Chem.* **272,** 19193–19198
33. Sun, L., Liang, C., Shirazian, S., Zhou, Y., Miller, T., Cui, J., Fukuda, J. Y., Chu, J. Y., Nematalla, A., Wang, X., Chen, H., Sistla, A., Luu, T. C., Tang, F., Wei, J., and Tang, C. (2003) *J. Med. Chem.* **46,** 1116–1119
34. Dong, B., Xu, L., Zhou, A., Hassel, B. A., Lee, X., Torrence, P. F., and Silverman, R. H. (1994) *J. Biol. Chem.* **269,** 14153–14158
35. Nakanishi, M., Goto, Y., and Kitade, Y. (2005) *Proteins* **60,** 131–138
36. Karaman, M. W., Herrgard, S., Treiber, D. K., Gallant, P., Atteridge, C. E., Campbell, B. T., Chan, K. W., Ciceri, P., Davis, M. I., Edeen, P. T., Faraoni, R., Floyd, M., Hunt, J. P., Lockhart, D. J., Milanov, Z. V., Morrison, M. J., Pallares, G., Patel, H. K., Pritchard, S., Wodicka, L. M., and Zarrinkar, P. P. (2008) *Nat. Biotechnol.* **26,** 127–132
37. Kerkela, R., Woulfe, K. C., Durand, J. B., Vagnozzi, R., Kramer, D., Chu, T. F., Beahm, C., Chen, M. H., and Force, T. (2009) *Clin. Transl. Sci.* **2,** 15–25
38. Luthra, P., Sun, D., Silverman, R. H., and He, B. (2011) *Proc. Natl. Acad. Sci. U.S.A.* **108,** 2118–2123
39. Malathi, K., Saito, T., Crochet, N., Barton, D. J., Gale, M., Jr., and Silverman, R. H. (2010) *RNA* **16,** 2108–2119
40. Yang, Y. L., Reis, L. F., Pavlovic, J., Aguzzi, A., Schäfer, R., Kumar, A., Williams, B. R., Aguet, M., and Weissmann, C. (1995) *EMBO J.* **14,** 6095–6106